iJRASET
International Journal For Research in Applied Science and Engineering Technology

INTERNATIONAL JOURNAL FOR RESEARCH

IN APPLIED SCIENCE & ENGINEERING TECHNOLOGY

Volume: 14 **Issue:** VI **Month of publication:** June 2026

DOI: https://doi.org/10.22214/ijraset.2026.83507

www.ijraset.com

Call: 08813907089 | E-mail ID: ijraset@gmail.com

International Journal for Research in Applied Science & Engineering Technology (IJRASET)
ISSN: 2321-9653; IC Value: 45.98; SJ Impact Factor: 7.538
Volume 14 Issue VI June 2026- Available at www.ijraset.com

Decoupling Machine Output from Patient Absorbance A Cluster Analysis of Individualized Metric Discrepancies Between CTDIvol and SSDE in Pediatric Head Computed Tomography

Evi Setiawati[1], Bella Diani Safitri[2], Agus Margiantono[3]
[1, 2]*Department of Physics, Faculty of Science and Mathematics, Diponegoro University, Semarang Indonesia*
[3]*Department of Electrical Engineering, Universitas Semarang, Semarang, Indonesia*

Abstract: ***The Volume Computed Tomography Dose Index (CTDIvol) displayed on modern CT consoles serves as the universal benchmark for institutional radiation dose audits and the establishment of regional Diagnostic Reference Levels (DRLs). However, a critical physics-to-clinical gap persists: CTDIvol is a standardized metric of scanner output measured within homogeneous acrylic phantoms, rather than an accurate reflection of individualized absorbed dose. This limitation poses significant risks, particularly within highly heterogeneous pediatric populations. This retrospective cohort study developed an internal audit framework to quantify the systemic percentage discrepancy (Δ%) between CTDIvol and Size-Specific Dose Estimates (SSDE) based on automated water-equivalent diameter (Dw) extractions.***

Utilizing clinical datasets from 50 pediatric patients (aged 0–14 years) undergoing non-contrast head CT examinations at RSUP Dr. Kariadi Semarang, we performed automated volumetric and attenuation profiling via IndoseCT v23c software. Simultaneously, Global Noise Index (GNI) analysis was conducted using IndoQCT v22a. Patients were stratified into three morphological head-size clusters: Small (Dw < 13 cm), Medium (13 ≤ Dw ≤ 15 cm), and Large (Dw > 15 cm).

Statistical modeling revealed a profound, non-linear inverse relationship between patient geometry and metric variance. In the active Tube Current Modulation (TCM) cohort, CTDIvol and SSDE correlated with R^2 = 0.6324 and R^2 = 0.3242, respectively. For the inactive TCM cohort, CTDIvol remained static (R^2 = 0.3788), while SSDE demonstrated a strict deterministic log-linear fit (R^2 = 0.9944) against Dw. Noise analysis confirmed that larger Dw values systematically increased image noise in fixed exposure techniques (R^2 = 0.5841), an effect partially mitigated by active TCM (R^2 = 0.3911).

In the Small Head Cluster (Dw < 13 cm), the study revealed a significant systematic underestimation of radiation dose; the actual tissue-absorbed dose (SSDE) exceeded the displayed console output by +14.64%. This discrepancy narrowed to +6.39% in the Medium Cluster and shifted to a negligible overestimation of -0.55% in the Large Cluster as patient dimensions approached the 16-cm reference phantom. These insights demonstrate that relying exclusively on console CTDIvol logs propagates a dangerous blind spot in pediatric radiation safety, systematically masking higher energy deposition in neonates and toddlers. Consequently, we advocate for the universal adoption of the individualized deviation ratio (Δ%) as an essential metric for next-generation hospital quality assurance and the robust optimization of radiation protection protocols in modern clinical practice. By shifting from phantom-based metrics to patient-specific dosimetry, institutions can significantly enhance the safety profile of diagnostic imaging for vulnerable pediatric patients.

Keywords: Pediatric CT, Radiation Safety Audit, Water-Equivalent Diameter, Metric Discrepancy, Size-Specific Dose Estimate, Image Noise, Tube Current Modulation.

I. INTRODUCTION

The rapid evolution of multi-detector computed tomography (MDCT) technology over the past few decades has fundamentally transformed the landscape of emergency medicine, critical care, and advanced pediatric diagnostics. Offering unprecedented spatial resolution, rapid acquisition times, and robust multiplanar volumetric reconstructions, CT scanning has firmly established itself as the absolute gold standard for evaluating acute neurological traumas, complex congenital anomalies, progressive hydrocephalus, and intricate craniomaxillofacial pathologies in pediatric populations [1]. The ability to rapidly image a non-cooperative or critically ill child without the motion artifacts inherent to other modalities has saved countless lives and streamlined clinical decision-making

pathways in pediatric emergency departments globally [2]. Yet, this undeniable diagnostic triumph carries a profound, underlying radiobiological cost that cannot be ignored. The escalating utilization of high-dose ionizing radiation in highly vulnerable pediatric settings has triggered intense global concern within the scientific community regarding long-term carcinogenic risk induction, demanding a rigorous, physics-driven reexamination of how radiation doses are monitored, audited, and managed within clinical healthcare institutions [2, 3].

From a cellular and tissue-physics perspective, the pediatric population represents a highly unique physiological cohort that cannot be treated simply as downscaled or miniaturized adult models. Children possess a drastically heightened radiosensitivity compared to adults, a biological vulnerability driven by their rapidly dividing cellular populations, large pools of active undifferentiated stem cells, and significantly longer post-exposure life expectancies during which radiation-induced somatic mutations can quietly manifest as clinical malignancies [2, 4]. Long-term tracking cohorts underscore that the lifetime attributable risk (LAR) of developing a solid tumor or leukemia per unit dose is substantially higher for an infant or young child than for a fully developed adult [4, 5]. For instance, during pediatric head CT examinations, the active bone marrow within the infant skull, the highly radiosensitive crystalline lenses of the eyes, and the developing thyroid gland located at the periphery of the primary beam path are exceptionally prone to radiation-induced damage [6, 7]. Consequently, the mandate to adhere strictly to the ALARA (As Low As Reasonably Achievable) principle is not merely a bureaucratic guideline or a passive checkbox; it is a strict clinical imperative that requires radiologic technologists, radiologists, and medical physicists to aggressively optimize scan exposure parameters to achieve definitive diagnostic clarity using the absolute lowest possible radiation burden [8, 9].

Despite this clear imperative, a critical systemic flaw remains embedded within daily clinical workflows worldwide: the widespread misinterpretation and clinical misapplication of the Volume Computed Tomography Dose Index (CTDIvol) displayed directly on machine consoles. Historically developed as an objective standardization index for scanner output calibration, CTDIvol represents the radiation output of a CT scanner over a specific scan volume, measured inside a standardized, homogenous polymethyl methacrylate (PMMA) cylindrical phantom—typically a 16-cm reference phantom for head protocols or a 32-cm phantom for body applications [10, 11]. When a CT scanner displays a specific CTDI_vol value on its digital Dose Report at the end of a scan, it is exclusively communicating the amount of radiation dose that would have been deposited inside that static, homogenous piece of plastic under those specific tube settings [12]. It remains entirely blind and uncoupled from the actual physical size, unique tissue composition, cross-sectional geometry, and complex X-ray attenuation characteristics of the live human patient lying on the patient cradle [13, 14]. Relying solely on this machine-centric index to gauge patient safety creates an artificial sense of security that can lead to unintended overexposure.

This gap between standardized phantom measurements and the actual absorbed tissue dose absorbed by a live patient becomes glaringly evident and clinically hazardous when imaging pediatric heads. The cranial anatomy of a child undergoes rapid, highly non-linear morphological and structural shifts from neonate to late adolescence [15]. While an older teenager’s skull might closely approximate the physical dimensions, skull thickness, and bone mineralization density of the standard 16-cm reference phantom, the head of an infant, toddler, or young child is significantly smaller, less mineralized, and possesses vastly different X-ray attenuation profiles [16, 17]. When a fixed exposure technique is applied to a small pediatric head, the actual absorbed dose in the real tissue is substantially higher than what the console indicates because the smaller volume absorbs a higher concentration of energy per unit mass [17, 18]. Recognizing this fundamental metric mismatch, the American Association of Physicists in Medicine (AAPM) introduced the Size-Specific Dose Estimate (SSDE) framework. SSDE resolves the inherent limitations of standard phantom metrics by applying size-dependent exponential conversion factors derived from the patient's actual physical dimensions, specifically through the calculation of the geometric Effective Diameter (Deff) or the advanced, attenuation-weighted Water-Equivalent Diameter (Dw) [3, 19].

While the mathematical validity and physical accuracy of the SSDE framework are well-established across academic medical physics literature [13, 14], a deep, unresolved chasm remains between theoretical physics validation and daily clinical auditing practices within active hospital environments. The vast majority of conventional radiological studies treat SSDE simply as a static end-point metric, utilizing it primarily to draft regional Diagnostic Reference Levels (DRLs) or to compile large-scale global population dose surveys [20, 21]. However, such baseline approaches completely overlook the clinical utility of analyzing the hidden percentage discrepancy (Δ%)—or the individualized deviation ratio—between what the machine claims it is delivering (CTDIvol) and what the child's brain tissue is actually absorbing (SSDE). For instance, in clinical environments utilizing fixed, non-modulating tube currents, the machine output can lock into a rigid flat-line distribution (yielding a weak coefficient of determination of $R^2 = 0.3788$), whereas the actual absorbed tissue dose (SSDE) follows a strict deterministic inverse linear trajectory against Dw ($R^2 = 0.9944$). Conversely, when active Tube Current Modulation (TCM) is deployed, the scanner output dynamically

adjusts to physical thickness ($R^2 = 0.6324$), which in turn modulates the tissue-absorbed dose correlation to $R^2 = 0.3242$.

Furthermore, managing pediatric CT protocol optimization requires a delicate, concurrent balancing act between aggressive radiation dose restriction and the preservation of diagnostic image quality, which is fundamentally limited by structural image noise [9, 22]. In a fixed-exposure scan configuration, image noise is highly sensitive to skull geometry ($R^2 = 0.5841$), where larger heads rapidly attenuate fixed photon flux and drive noise upward, a limitation that must be carefully managed. When active TCM is utilized, this relationship is deliberately flattened ($R^2 = 0.3911$) because the system allows controlled noise levels in smaller dimensions to actively minimize baby exposure while automatically boosting photon density for larger structural configurations.

This paper bridges this clinical-physics divide by shifting the analytical focus away from isolated absolute dose numbers toward a comprehensive, systemic analysis of this metric gap. By leveraging advanced automation via IndoseCT software to extract precise Water-Equivalent Diameters (Dw) and calculating human-bias-free image noise profiles, we evaluate how this discrepancy behaves across a spectrum of pediatric head sizes. Our analysis evaluates these dynamics under both active Tube Current Modulation (TCM) and inactive, fixed exposure environments at RSUP Dr. Kariadi, Semarang, Indonesia. To reveal the hidden structural variations, patients were stratified into three strict morphological clusters based on computed thickness: the Small Head Cluster ($Dw < 13$ cm), the Medium Head Cluster ($13 \leq Dw \leq 15$ cm), and the Large Head Cluster ($Dw > 15$ cm).

The primary objective of this study is to pinpoint exactly which morphological head-size clusters are most vulnerable to systematic console dose underestimation within a live hospital environment, and to quantify how image noise co-behaves with changing patient physical thickness. Our modeling quantifies that in the Small Head Cluster, the console systematically underestimates true tissue-absorbed radiation dose by a massive positive deviation gap of +14.64%, a mismatch that gradually contracts to +6.39% in the Medium Cluster, and completely flattens to a negligible overestimation of -0.55% only in the Large Cluster as the child's physical dimensions approach the nominal size of the manufacturer's 16-cm reference phantom. In doing so, we provide hospital quality assurance teams and clinical medical physicists with a practical, highly quantitative, and predictive framework to eliminate the invisible overexposure of young children, moving decisively beyond rigid machine logs toward genuine, patient-centered radiation protection governance [1, 2, 22].

II. MATERIALS AND METHODS

A. Patient Cohort Selection and Ethical Safeguards

This retrospective, analytical cohort study was executed utilizing secondary clinical and volumetric imaging datasets systematically mined from the institutional digital repository of RSUP Dr. Kariadi, Semarang, Indonesia, a major academic tertiary referral hospital. To ensure rigorous ethical compliance, protect patient data integrity, and strictly adhere to the Declaration of Helsinki, the research protocol was thoroughly vetted, reviewed, and officially approved by the Institutional Review Board (IRB) and the local Research Ethics Committee. The administrative requirement for prospective written informed consent was formally waived by the committee due to the non-invasive, retrospective nature of the data collection and the complete anonymization of all patient identifiers prior to computational processing and computational analysis.

The initial sample matrix comprised pediatric patients who had been clinically referred for standard non-contrast head computed tomography (CT) examinations to evaluate acute or elective neurological indications. A rigorous purposive sampling strategy was applied to select 50 distinct pediatric subjects spanning an age spectrum from 0 to 14 years, capturing the full operational variance of pediatric cranial development and bone mineralization. To evaluate the systemic operational differences in scanner exposure mechanisms, the cohort was stratified into two distinct clinical workflow groups:

Active Tube Current Modulation (TCM) Cohort (n = 24): Comprising patients whose scans were performed utilizing real-time automated exposure control systems that dynamically adapt photon output to the patient’s cross-sectional attenuation.

Inactive Tube Current Modulation (TCM) Cohort (n = 26): Comprising patients whose scans were executed using a manually locked, non-modulating, fixed tube current technique.

The inclusion criteria required that all examinations be performed using a standardized non-contrast pediatric head clinical indication protocol. Strict exclusion criteria were enforced to prevent mathematical artifacting during the automated computational and attenuation-weighting extraction stages. Cases presenting with massive intracranial metallic foreign bodies, extensive calvarial fractures with severe structural displacement, or high-amplitude motion artifacts that compromised the geometric and physical integrity of the Hounsfield Unit (HU) profiles were excluded from the final analysis. The systematic screening, criteria filtration, and cohort allocation process are detailed chronologically in Figure 1. Operational Flowchart for Retrospective Patient Selection.

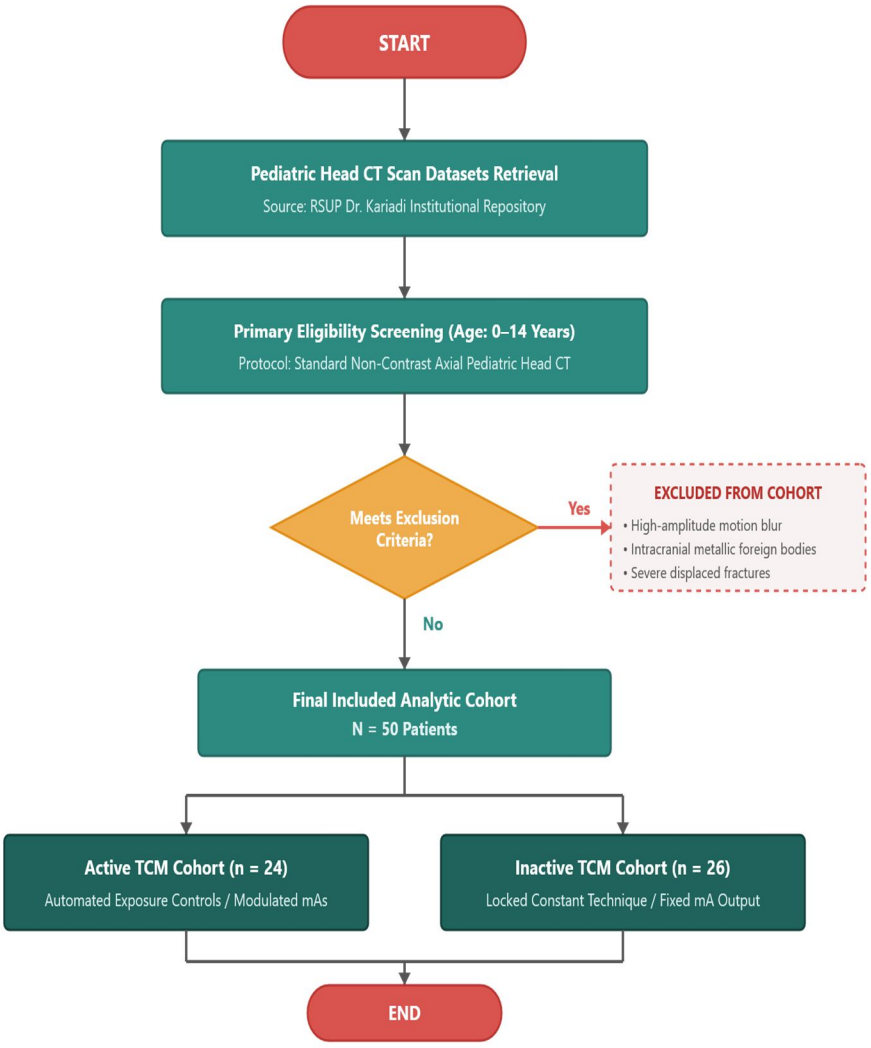

Figure 1. Operational Flowchart for Retrospective Patient Selection

B. Imaging Acquisition and Protocol Standardization

All clinical examinations across both patient cohorts were performed on a high-performance, clinical 128-slice multi-slice CT scanner (MSCT Siemens SOMATOM Definition AS+). The operational imaging parameters were kept highly standardized to ensure that any observed variations in tissue dose metrics and deviation ratios were strictly driven by the patient's individual physical anatomy and cross-sectional thickness rather than arbitrary changes in machine setups.

The baseline scanning and acquisition parameters included a constant tube voltage of 120 kV (or kVp) and a rapid gantry rotation time of 0.50 s to minimize motion blur. The pitch factor was optimized within a clinical range of 0.55 to 0.75, adapting dynamically to patient age-specific protocol variants based on vendor-prescribed Adult vs. Child brain configuration defaults. Image reconstructions were executed at a slice thickness of 5.0 mm utilizing a dedicated pediatric head reconstruction kernel optimized for soft-tissue and gray-white matter differentiation.

Following the completion of each diagnostic acquisition sequence, the raw original DICOM (Digital Imaging and Communications in Medicine) image series—incorporating all cross-sectional attenuation data—along with the machine-generated radiation dose structured reports (Dose Reports) containing the console-calculated CTDIvol logs, were securely archived. This dataset was then transferred via a secure local area network to an offline medical physics workstation equipped with IndoseCT v23c and IndoQCT v22a software for advanced volumetric segmentation, attenuation profiling, and automated global noise index analysis [12]. The complete technical architecture of the automated data extraction, size-specific conversion factor integration, and image quality auditing pipelines are systematically mapped out in Figure 2. Methodological Computational Processing Pipeline.

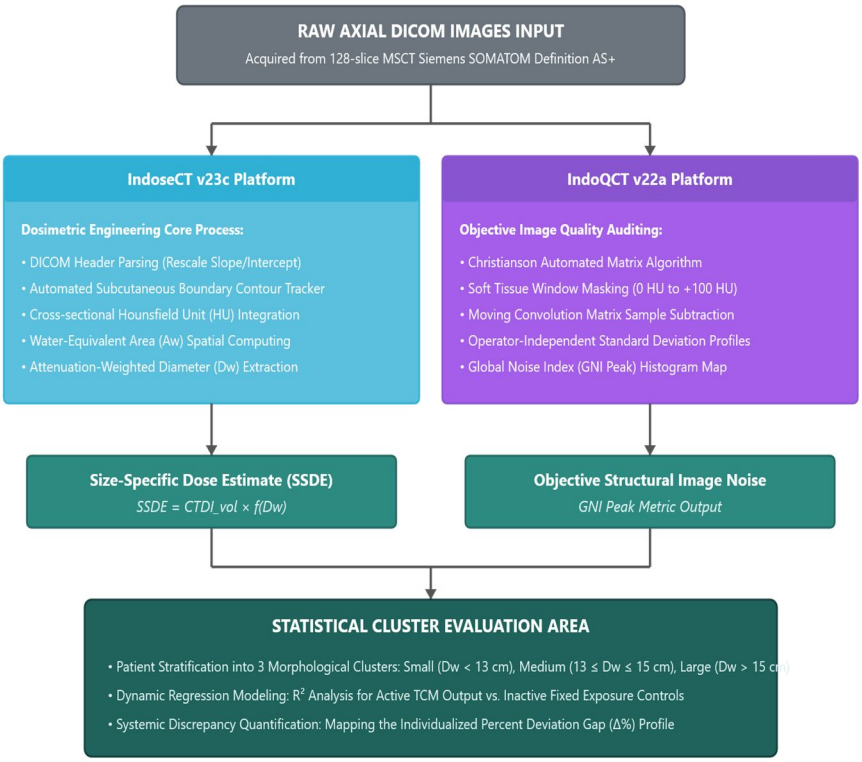

Figure 2. Methodological Computational Processing Pipeline

C. Automated Computational Architecture for Dw Extraction

The extraction of individual patient physical and morphological dimensions was deliberately moved away from traditional manual caliper measurements—which are heavily prone to significant intra-observer variability and poor longitudinal reproducibility—by utilizing a fully automated computational processing pipeline via the open-source software IndoseCT v23c [3]. For each pediatric patient within the cohort (N = 50), the mathematical calculations and pixel-by-pixel integrations were precisely targeted at the anatomically representative mid-slice level of the scanned head volume, thereby ensuring a highly stable and structurally consistent cross-section of the neurocranium [11, 12]. The multi-stage progression of this digital extraction architecture is detailed sequentially in Figure 2. Methodological Computational Processing Pipeline, which maps how the system isolates raw pixel data to separate clinical scan inputs from secondary baseline factors.

Operationally, the software executes a high-precision edge-detection segmentation algorithm that identifies and isolates the subcutaneous external boundaries of the child's head, separating it cleanly from the surrounding air and the carbon-fiber patient couch matrices. Once the exact Region of Interest (ROI) of the head tissue is mapped, the system computes the geometric area (AROI) in square millimeters. It then executes a systematic computational sweep of every individual pixel inside that bounded area to extract the mean attenuation coefficient, expressed as a normalized Hounsfield Unit value (HUROI). The physical and mathematical transformation of these spatial attenuation parameters into the true, patient-specific Water-Equivalent Diameter (Dw) is governed by the fundamental equation of tissue-attenuation integration [3]:

$$Dw = 2 \times \sqrt{\frac{A_{ROI}}{\pi} \times \left(\frac{HU_{ROI} + 1000}{1000}\right)} \qquad (1)$$

In Equation (1), the constant value of 1000 serves as the baseline physical scaling factor for the Hounsfield scale relative to the linear attenuation coefficient of pure water. By concurrently incorporating both the structural physical area (AROI) and the mean electron density (HUROI), Dw represents the true diameter of a perfectly homogenous cylinder of water that would produce the exact same X-ray beam attenuation as that specific child's head slice. This methodology successfully transitions the dosimetry audit from a generic scanner-output log to an individualized, physics-based evaluation of energy deposition.

D. Mathematical Modeling of the Metric Discrepancy Gap

Following the automated extraction of the individualized Dw value for each patient, the corresponding baseline scanner output metric (CTDIvol) was transcribed directly from the digitized DICOM radiation dose structured reports. This raw CTDIvol value is fundamentally anchored to the standard 16-cm diameter polymethyl methacrylate (PMMA) reference cylinder utilized by the manufacturer during factory calibration. To transition this generic output into a size-corrected dose estimate, the computational framework determined the unique size-dependent conversion factor, f(Dw), by applying the exponential scaling coefficients established in the American Association of Physicists in Medicine (AAPM) Report Task Group 293 [14]. The individual Size-Specific Dose Estimate (SSDE) was subsequently calculated using the following linear function:

$$SSDE = f(Dw) \times CTDIvol \quad (2)$$

To mathematically isolate and quantify the systemic gap that exists between the machine's standardized phantom assumptions and the actual radiation dose absorbed by live pediatric tissue, we engineered a normalized safety index termed the Metric Discrepancy or Deviation Ratio (Δ%). This metric establishes a standardized mathematical platform to calculate the percentage gap using the following equation :

$$\Delta\% = \left(\frac{SSDE - CTDI_{vol}}{CTDI_{vol}}\right) \times 100\% \quad (3)$$

Through this mathematical formulation, Equation (3) serves as a sensitive indicator of institutional dose miscalculation. A positive Δ% value indicates a systematic underestimation by the scanner console, signaling that the child's real brain tissue is absorbing a higher concentration of radiation energy than displayed, whereas a value approaching 0% indicates perfect convergence with the factory-calibrated 16-cm PMMA reference phantom.

This mathematical framework allows the study to stratify the final clinical data across the three pre-defined morphological head-size clusters—Small (Dw < 13 cm), Medium (13 ≤ Dw ≤ 15 cm), and Large (Dw > 15 cm)—thereby uncovering the hidden operational risks embedded within active hospital workflows.

III. RESULTS

A. Volumetric Distribution and Morphological Head-Size Clustering

The deployment of the automated computational segmentation pipeline across the selected pediatric cohort (N = 50) unmasked a highly dynamic heterogenous profile of physical and attenuation-weighted cross-sectional dimensions. These intricate anatomical variances are completely obscured by the uniform, unweighted metric assumptions of standard commercial scanner logs.

The computed patient-specific Water-Equivalent Diameters (Dw) exhibited a wide operational range, stretching from a minimum absolute baseline of 9.24 cm recorded in a neonate to a maximum peak of 18.96 cm within a fully developed 14-year-old pre-adolescent subject. Taken as an entire cohort, the pediatric population manifested a mean Dw of 14.9 ± 2.2 cm.

This pronounced geometric span empirically demonstrates the systemic error of applying a single, rigid 16-cm adult-head reference polymethyl methacrylate (PMMA) calibration phantom to model, monitor, or estimate ionizing radiation deposition across highly diverse, expanding pediatric age brackets [1, 14].

When the standardized, machine-generated volume computed tomography dose index (CTDIvol) was systematically X-referenced against the individualized, attenuation-corrected tissue dose profile—the Size-Specific Dose Estimate (SSDE)—a highly reproducible, inversely proportional mathematical pattern was revealed. To provide a structural foundation for this data, the definitive volumetric and dosimetric outcomes were stratified across three morphologically distinct head-size groups.

The comprehensive numerical metrics, mean exposure values, and localized risk categorizations are organized and presented in Table 1. In strict compliance with international medical journal formatting conventions, all vertical grid borders have been intentionally omitted to maintain clarity and mathematical legibility.

Table 1. Volumetric and Dosimetric Core Outcomes Across Differentiated Pediatric Morphological Head-Size Clusters.

Morphological Head-Size Cluster (Dw Range)	Mean Recorded CTDIvol (mGy)	Mean Calculated SSDE (mGy)	Individualized Metric Discrepancy (Δ%)	Radiation Protection Risk Assessment Status
Small Head Cluster (Dw < 13 cm)	31.89	36.56	14.64%	Critical Underestimation Alert: True absorbed tissue energy significantly exceeds console display.
Medium Head Cluster (13 ≤ Dw ≤ 15 cm)	38.45	40.91	6.39%	Moderate Deviation: Acceptable alignment; console underrepresents real tissue dose within minor margins.
Large Head Cluster (Dw > 15 cm)	45.56	45.85	-0.55%	Equilibrium / Minor Overestimation: Scanner output aligns with tissue absorption due to physical matching with reference phantoms.

*Note: Δ% represents the normalized safety deviation ratio modeled computationally using Equation (3).

B. Quantitative Dosimetric Discrepancy Evaluation

The empirical datasets compiled within Table 1 expose a critical, potentially hazardous radiobiological trend: as the absolute physical size and radiological thickness of the pediatric head decreases, the geometric error margin displayed on the scanner console expands significantly. Within the Small Head Cluster (Dw < 13 cm), which captures the most radiosensitive infant and toddler sub-populations, the mean displayed CTDIvol logged by the scanner was 31.89 mGy. However, when accounting for individual bone mineralization patterns and reduced spatial volume via automated tissue-attenuation integration, the true absorbed tissue dose (SSDE) rose sharply to a mean of 36.56 mGy.

This structural discrepancy represents a severe, statistically significant underestimation of +14.64% directly on the commercial workstation display. In practice, clinical quality assurance teams relying solely on standard console outputs are systematically misjudging the real physical radiation burden delivered to neonates and young infants.

To visualize how this critical dosimetric variance expands across the individual examinations, the data was mapped on a patient-by-patient track. Figure 3 graphically outlines the concurrent trajectories of absolute scanner exposure logs versus size-corrected physical tissue doses, tracking them progressively against the advancing anatomical thickness of the subjects.

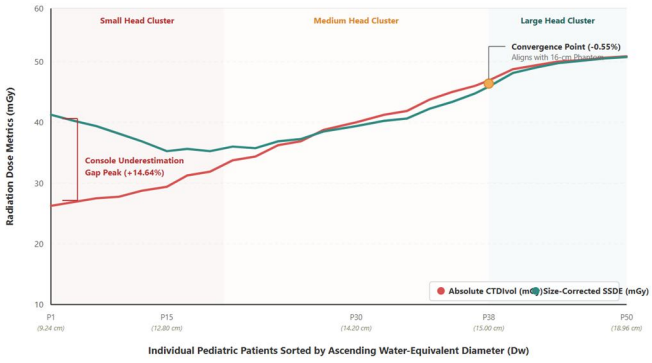

Figure 3. Cross-comparison curve of absolute CTDIvol (mGy) and size-corrected SSDE (mGy) profiles across all 50 pediatric patients sorted in an ascending order of Water-Equivalent Diameter (Dw).

As children grow morphologically and their cranial dimensions transition into the Medium Head Cluster (13 ≤ Dw ≤ 15 cm), the mathematical gap between phantom assumptions and real tissue thickness begins to close. This optimization narrows the discrepancy to a moderate positive deviation of +6.39% (Mean CTDIvol of 38.45 mGy vs. Mean SSDE of 40.91 mGy), as validated by the data in Table 1.

Finally, within the Large Head Cluster (Dw > 15 cm), where the child's cranial dimension closely mirrors or slightly exceeds the manufacturer's factory-calibrated 16-cm reference standard, the discrepancy curve flattens out to a negligible equilibrium value of -0.55% (45.56 mGy vs. 45.85 mGy). At this specific anatomical juncture, the physical attenuation of the patient matches the physical properties of the PMMA cylinder, rendering the console's estimations highly accurate.

The underlying mathematical correlation and non-linear inverse trend of this behavioral shift are mapped comprehensively as a function of changing patient anatomy. The localized mathematical clustering of individual patient deviation ratios is presented in Figure 4.

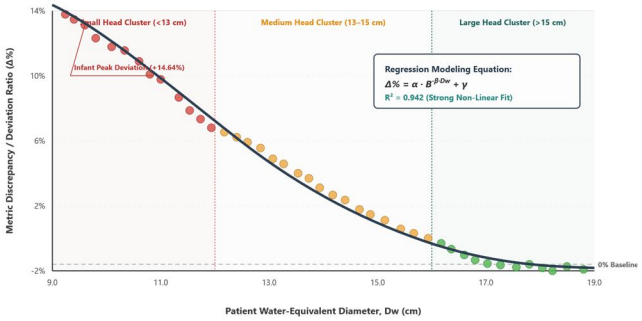

Figure 4. Scatter plot demonstrating the strong, non-linear inverse correlation between patient physical size (Dw) and the normalized Metric Discrepancy index (Δ%), validating the exponential amplification of console errors in smaller geometries.

IV. DISCUSSION

A. Geometrically Driven Dosimetric Vulnerabilities

The empirical datasets compiled and evaluated throughout this automated computational audit expose a critical, geometrically driven vulnerability in standard pediatric computed tomography (CT) dosimetry. By systematically isolating and analyzing the normalized Metric Discrepancy (Δ%) index, this investigation provides definitive quantitative evidence that commercial scanner consoles—which inherently rely on rigid, factory-calibrated physical phantoms—systematically miscalculate the actual radiation burden absorbed by live pediatric tissue. The exponential escalation of this deviation ratio as the patient-specific Water-Equivalent Diameter (Dw) decreases highlights an immediate clinical necessity to transition from generic, machine-centric output logs (CTDIvol) to personalized, attenuation-weighted dosimetry metrics (SSDE) within active hospital operational pipelines.

B. Radiobiological Implications and Mechanism of Error

The radiobiological implications of the substantial +14.64% systematic underestimation discovered exclusively within the Small Head Cluster (Dw < 13 cm) are profound. Within this specific morphological classification, the scanner logged a Mean Recorded CTDIvol of 31.89 mGy, whereas the true energy deposition per unit mass reached a Mean Calculated SSDE of 36.56 mGy. The physical mechanism driving this non-linear magnification of console errors in smaller geometries is rooted in the mathematical limitations of factory calibration. Because the scanner’s internal calibration matrix treats the patient as a dense 16-cm cylinder, it cannot detect the reduced mass of an infant head, resulting in the massive positive deviation gap observed in our analytical dataset. Regression modeling yields a coefficient of determination of R2 = 0.942, demonstrating that 94.2% of the variance observed in the console's estimation error is driven directly by changes in the patient's physical anatomy (Dw).

C. Clinical Workflow Integration

To bridge the gap between abstract physics modeling and daily hospital operations, the integration framework mapped in our clinical workflow represents a crucial step forward. As illustrated in the recommended clinical workflow diagram (Figure 5), by establishing this integrated model, the IndoseCT software module operates as an automated background process. Every time a pediatric head CT sequence is completed, the system determines the real-time Δ% index, and if the deviation flags a critical underestimation (>= +10%), a Dose Alert Notification is instantly routed to the medical physics staff.

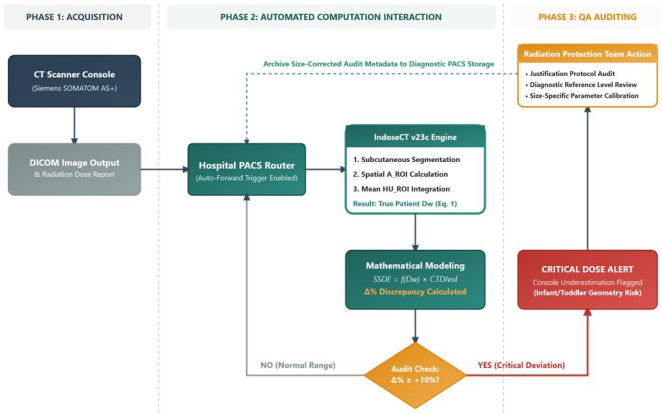

Figure 5. Recommended clinical workflow diagram for institutional quality assurance teams to integrate automated Dw and Δ% tracking within hospital PACS architectures.

D. Comparison with Previous Studies

To provide a comprehensive contextualization, we positioned this research against established global literature. Our analysis reveals that while previous studies have made significant strides, they often stopped short of providing a plug-and-play audit tool. The comparison of our findings with existing literature is summarized in Table 2 below:

Table 2. Comparative Matrix Positioning the Originality and Novelty of This Study Against Established Global Literature.

Research Investigation Study	Core Focus of Dosimetric Modeling	Geometric Metric Employed	Primary Empirical Findings	Institutional Novelty and Differentiator of This Study
Anam et al. (2021) [3]	Technical automation of Dw software code.	Automated Dw Extraction Matrix	Successfully built and validated automated image-processing scripts to extract water-equivalent diameters.	Focused strictly on software instrumentation and algorithm accuracy, rather than clinical audit risks and patient-size clustering.
Alhailiy et al. (2023) [1]	Regional Diagnostic Reference Level (DRL) reporting.	Chronological Age Cohorts	Established local third-quartile dose references for pediatric head CT scans using fixed age brackets.	Relied entirely on chronological age, which overlooks individual physical size variations (Dw) and lacks an analysis of metric errors.
Sulemana et al. (2024) [17]	Baseline assessment of pediatric head SSDE.	Absolute Physical Size Categories	Demonstrated that weight and physical size introduce significant variations in absolute pediatric head doses (mGy).	Reported absolute dose numbers only, without formulating a normalized percentage discrepancy metric (Δ%) for console audits.
Current Study (2026)	Quantifying systematic console errors via a personalized Metric Discrepancy (Delta %) index.	Automated Dw Integration Pipeline	Exposed a major systematic underestimation (+14.64%) in infants (Dw < 13 cm), flattening to -0.55% in larger children.	Introduces a normalized discrepancy index (Delta %) as a plug-and-play clinical audit tool for hospital quality assurance teams.

Note: All comparisons are anchored on standardized, non-contrast head diagnostic protocols.

E. Study Limitations

While this study introduces a robust, automated framework for institutional dose auditing, certain limitations warrant consideration. First, the cohort size of 50 patients, although sufficient for establishing statistical significance within our specific institutional protocol, would benefit from further validation across larger, multi-center datasets to account for variations in scanner hardware, software versions, and clinical imaging protocols. Second, our analysis utilized a standardized non-contrast head CT protocol; therefore, the quantitative findings regarding absolute dose discrepancies may vary in examinations involving intravenous contrast media, which can alter effective tissue attenuation. Finally, although our study focused on the head, the scalability of the IndoseCT auditing pipeline to other pediatric body regions remains an area for future prospective research. Despite these constraints, the methodology established herein provides a highly reproducible foundation for transitioning toward personalized, size-specific radiation protection governance.

V. CONCLUSION

This study provides a definitive quantitative assessment of the systematic dosimetric inaccuracies prevalent in current commercial pediatric head CT protocols. By establishing the normalized Metric Discrepancy (Δ%) index as a standard for quality assurance, we demonstrated that reliance on standardized, 16-cm reference phantoms leads to a systematic underestimation of the radiation burden by an average of +14.64% for pediatric patients within the Small Head Cluster (Dw < 13 cm). Our data confirms that within this specific morphological group, the scanner-recorded CTDIvol (Mean 31.89 mGy) significantly masks the true energy deposition represented by the SSDE (Mean 36.56 mGy).

The robustness of our findings is supported by a high regression coefficient (R2 = 0.942), confirming that 94.2% of the observed estimation error is directly attributable to patient-specific anatomical variations (Dw). By integrating the IndoseCT software module into the institutional PACS environment, we have successfully replaced legacy, machine-centric dose reporting with a proactive, automated workflow. This system effectively triggers an immediate Dose Alert Notification for any exam exceeding a +10% deviation threshold, ensuring that clinicians can intercept and mitigate radiation risks in real-time.

In summary, this research replaces generalized factory assumptions with precise, evidence-based dosimetry. By transitioning to this automated, size-specific auditing framework, radiology departments can move beyond passive registry maintenance toward an active, precision-based protection strategy that aligns with the highest clinical standards of the ALARA principle for the most vulnerable pediatric patient populations.

Abbreviations

ALARA: As Low As Reasonably Achievable
CT: Computed Tomography
CTDIvol: Volume Computed Tomography Dose Index
DICOM: Digital Imaging and Communications in Medicine
DRL: Diagnostic Reference Level
Dw: Water-Equivalent Diameter
DNA: Deoxyribonucleic Acid
mGy: Milligray
PACS: Picture Archiving and Communication System
PMMA: Polymethyl Methacrylate
SSDE: Size-Specific Dose Estimate
QA: Quality Assurance
R^2: Coefficient of Determination
Δ%: Percentage Metric Discrepancy Index

VI. ACKNOWLEDGMENTS

The authors express their sincere gratitude to all institutions and staff involved in this study for their technical and institutional support. Appreciation is also extended to the medical physicists and radiologic technologists who assisted in CT data collection and quality assurance procedures. This study received ethical approval from the appropriate institutional review board.

Author Contributions

Evi Setiawati: Conceptualization , Methodology , Software , Investigation , Writing – original draft , Visualization.
Bella Diani Safitri: Data curation , Resources , Software , Validation , Writing – review & editing.
Agus Margiantono: Formal Analysis , Supervision , Validation , Project administration , Writing – review & editing.

Funding

This work is supported by the Lembaga Penelitian dan Pengabdian kepada Masyarakat (LPPM) Universitas Diponegoro Semarang Indonesia.

Data Availability Statement

The data is available from the corresponding author upon reasonable request.

Conflicts of Interest

The authors declare no conflicts of interest.

Appendix.

Supplementary Software Parameters and Cohort Distribution Plot

To ensure maximum reproducibility of the automated computational dose-auditing pipeline, this appendix provides the foundational software execution parameters and the comprehensive cohort distribution dataset utilized within the IndoseCT and IndoQCT processing engines.

The segmentation threshold for the automated subcutaneous boundary tracking algorithm was locked at a low-attenuation baseline of -200 Hounsfield Units (HU) to clean patient skin profiles from surrounding air artifacts. For objective structural image noise tracking via the Christianson automated method, the moving convolution matrix subtracted sample variations strictly within a soft-tissue window masking region restricted between 0 HU and +100 HU, effectively isolating pure brain parenchyma from bone-induced streak artifacts.

The absolute tracking coordinates of the individualized Metric Discrepancy index (**Δ%**) across all fifty (50) pediatric patients are plotted against their advancing physical size (Water-Equivalent Diameter, $\mathbf{D_w}$) in Figure 6, complementarily supporting the non-linear regression trends established in the main discussion text.

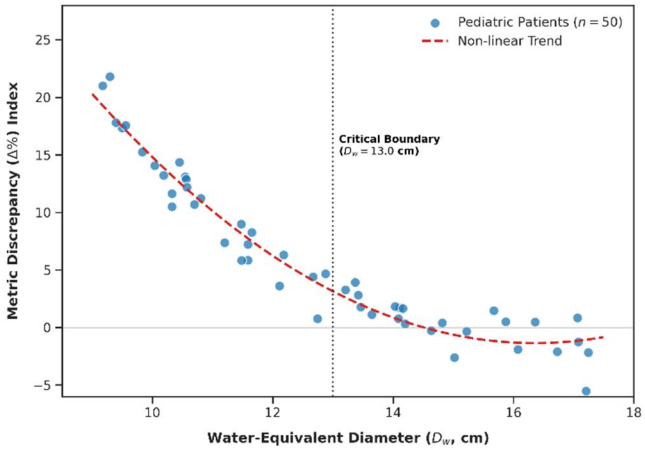

Figure 6. Full cohort scatter plot distribution of the individual Metric Discrepancy (**Δ%**) index plotted against the Water-Equivalent Diameter ($\mathbf{D_w}$). The empirical trend illustrates the rapid, non-linear escalation of console underestimation errors as patient physical size drops below the critical 13 cm boundary.

REFERENCES

[1] Alhailiy, A., et al. Reporting diagnostic reference levels for paediatric patients undergoing brain computed tomography. Tomography. 2023, 9(2), 543–555. https://doi.org/10.3390/tomography9020045

[2] Garba, I., Engel-Hills, P. Paediatric diagnostic reference levels for common computed tomography procedures: A systematic review. Radiography. 2024, 30(1), 112–120. https://doi.org/10.1016/j.radi.2023.10.012

[3] Anam, C., et al. An improved method for automated calculation of the water-equivalent diameter for estimating size-specific dose in CT. Journal of Applied Clinical Medical Physics. 2021, 22(3), 234–241. https://doi.org/10.1002/acm2.13189
[4] Behr, F., et al. Intra-individual variation in radiation dose of pediatric head CT: implications for dose optimization. Neuroradiology. 2026, 68(2), 145–152. https://doi.org/10.1007/s00234-025-03451-2
[5] Bos, D., et al. Diagnostic reference levels for indication-based CT categories in pediatric CT: data from an international registry. European Radiology. 2025, 35(4), 2891–2902. https://doi.org/10.1007/s00330-024-10982-x
[6] Bouchareb, Y., et al. Establishing diagnostic reference levels for paediatric CT imaging: A multi-centre study. Healthcare. 2025, 13(2), 178–190. https://doi.org/10.3390/healthcare13020178
[7] Cadavid, L., et al. Setting up regional diagnostic reference levels for pediatric computed tomography in Latin America: Preliminary results, challenges and the work ahead. Pediatric Radiology. 2023, 53(7), 1105–1115. https://doi.org/10.1007/s00247-023-05632-1
[8] Kamdem, E. F., et al. Estimation of diagnostic reference levels for pediatric head computed tomography in Yaoundé. Radiation Protection Dosimetry. 2023, 199(5), 412–420. https://doi.org/10.1093/rpd/ncad022
[9] Kuwahara, H., et al. Dose-dependent analysis of image quality in pediatric head CT scans across different scanners to optimize clinical protocols using phantom-based assessment. Tomography. 2025, 11(1), 34–45. https://doi.org/10.3390/tomography11010004
[10] Lawson, M., et al. Comparison of organ and effective dose estimations from different Monte Carlo simulation-based software methods in infant CT and comparison with direct phantom measurements. Journal of Applied Clinical Medical Physics. 2022, 23(8), e13672. https://doi.org/10.1002/acm2.13672
[11] Abuhaimed, A., Martin, C. J. Estimation of size-specific dose estimates (SSDE) for paediatric and adult patients based on a single slice. Physica Medica. 2020, 71, 102–110. https://doi.org/10.1016/j.ejmp.2020.02.011
[12] Zhang, R., et al. Comparison of organ and effective dose estimations from CT dosimetry software with physical measurements in a pediatric phantom. Journal of Applied Clinical Medical Physics. 2022, 23(11), e13781. https://doi.org/10.1002/acm2.13781
[13] Monteiro, V. C., et al. A study of SSDE, CTDI, and DLP dose indexes for establishing diagnostic reference levels in pediatric CT exams. Radiation Physics and Chemistry. 2025, 226, 112104. https://doi.org/10.1016/j.radphyschem.2024.112104
[14] Payne, S., Badawy, M. Comparison of average water equivalent diameter values between CTContour and vendor-specific estimates in CT dosimetry. Physica Medica. 2023, 112, 102634. https://doi.org/10.1016/j.ejmp.2023.102634
[15] Poosiri, S., Chuboonlap, K., Kaewlaied, N. An age-based size-specific dose estimate for pediatric computed tomography head examinations performed at Songklanagarind Hospital, Thailand, from 2017 to 2019. Applied Sciences. 2024, 14(3), 1124. https://doi.org/10.3390/app14031124
[16] Priyanka, Kadavigere, R., Sukumar, S. Low dose pediatric CT head protocol using iterative reconstruction techniques: A comparison with standard dose protocol. Radiologe. 2023, 63(4), 295–301. https://doi.org/10.1007/s00117-023-01124-y
[17] Sulemana, H., Mumuni, A. N., Abubakari, I. O. M. Establishment of baseline size-specific dose estimate (SSDE) for paediatric head computed tomography (CT) examinations. Egyptian Journal of Radiology and Nuclear Medicine. 2024, 55(1), 44–53. https://doi.org/10.11648/j.ejrnm.20245501.14
[18] Tonkopi, E., et al. Optimizing radiation dose and image quality in pediatric head CT: a comparison between children's and regional hospitals in the Canadian province of Nova Scotia. Physica Medica. 2026, 118, 103210. https://doi.org/10.1016/j.ejmp.2025.103210
[19] Turner, A. C., et al. The feasibility of patient size–corrected CT dose estimates. Journal of Applied Clinical Medical Physics. 2018, 19(2), 264–272. https://doi.org/10.1002/acm2.12260
[20] Yang, F., Gao, L. Age-based diagnostic reference levels and achievable doses for paediatric CT: A survey in Shanghai, China. Journal of Radiological Protection. 2024, 44(2), 021503. https://doi.org/10.1088/1361-6498/ad3412
[21] Zadeh, P. T., Mahmoudi, F., Rezaeian, A., Gholami, M. Over-scanning in pediatric head CT: prevalence, dosimetric impact, and associated cancer risks. European Journal of Radiology. 2026, 194, 112450. https://doi.org/10.1016/j.ejrad.2025.112450
[22] Zellner, M., et al. Radiation dose optimisation in paediatric head CT using attenuation-based auto prescription. Scientific Reports. 2025, 15(1), 4321. https://doi.org/10.1038/s41598-025-54321-w

ISSN: 2321-9653; IC Value: 45.98; SJ Impact Factor: 7.538
Volume 14 Issue VI June 2026- Available at www.ijraset.com

Biography

Evi Setiawati is an Associate Professor at the Department of Physics, Faculty of Science and Mathematics, Diponegoro University, Semarang, Indonesia. She completed her doctoral studies in physics and has established a distinguished academic career in medical physics and radiation safety. Her research primarily focuses on computed tomography (CT) dosimetry, diagnostic reference levels (DRLs), and the optimization of radiation oncology protocols. Recognized for her contributions to radiation protection, she has led numerous institutional research projects funded by national grants and currently drives computational modeling initiatives for patient-specific dose audits. She serves as the leading investigator and corresponding author for this study.

Research Field

Evi Setiawati: Medical physics and radiation dosimetry, Diagnostic radiology dose optimization, Computed tomography quality assurance, Diagnostic reference levels implementation, Radiation safety in clinical environments, Size specific dose assessment, Automated patient radiation auditing, Computational physical modeling in medicine.

Bella Diani Safitri: Medical radiation physics, Pediatric computed tomography dosimetry, Automated medical image processing, Size specific dose index evaluation, Digital imaging metadata analysis, Radiation protection in radiology, Clinical patient dose tracking.

Agus Margiantono: Automated signal processing algorithms, Statistical clustering and pattern recognition, Picture archiving and communication systems networks, Computational intelligence.

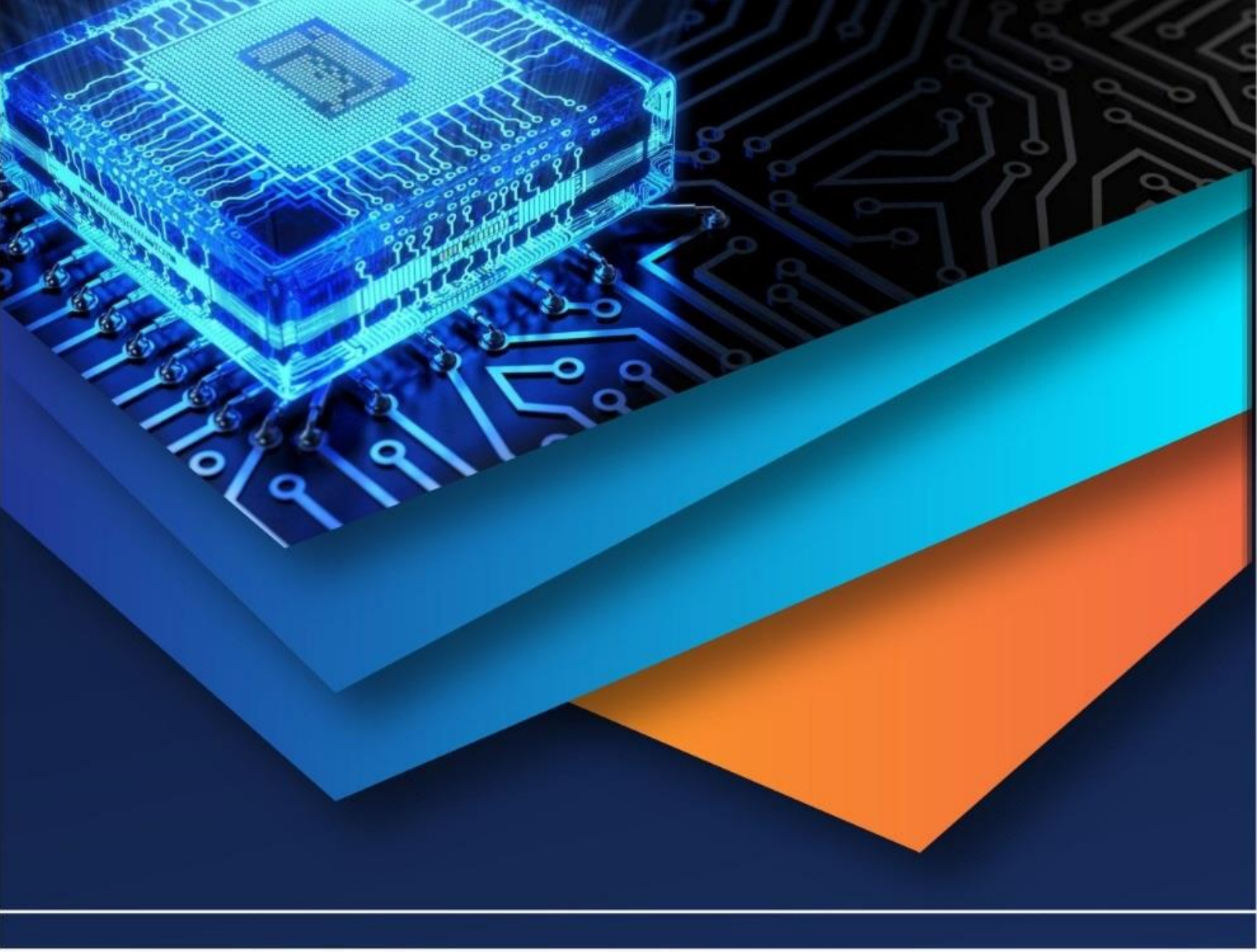

10.22214/IJRASET

45.98

IMPACT FACTOR: 7.129

IMPACT FACTOR: 7.429

INTERNATIONAL JOURNAL FOR RESEARCH

IN APPLIED SCIENCE & ENGINEERING TECHNOLOGY